Identification of Therapeutic Vulnerabilities in Small Cell Neuroendocrine Prostate Cancer

Alexandra N. Corella[1,2], Ma Victoria Andrea Cabiliza Ordonio[1,2], Ilsa Coleman[1,2], Jared M. Lucas[1,2], Arja Kaipainen[1,2], Holly M. Nguyen[3], Daniel Sondheim[3], Lisha G. Brown[3], Lawrence True[4], John Lee[1,2], David MacPherson[1], Paul Nghiem[2,5], Roman Gulati[6], Colm Morrissey[3], Eva Corey[3]*, Peter S. Nelson[1,2,4]*

Divisions of [1]Human Biology, [2]Clinical Research, and [6]Public Health Sciences, Fred Hutchinson Cancer Research Center, Seattle, WA, [3]Department of Urology, [4]Pathology and [5]Dermatology, University of Washington, Seattle, WA.

Running Title: Therapeutic targets in neuroendocrine prostate cancer

Keywords: prostate cancer, neuroendocrine, small cell, BCL2, WEE1

Conflicts of Interest: Peter Nelson has served as a consultant/advisory board member for Janssen and Astellas. The other authors declare no conflicts of interest.

***Correspondence to:**

Eva Corey
Department of Urology
Mailstop 356510
University of Washington
Seattle, WA 98195
Email: ecorey@uw.edu
Telephone: 206-543-1461

Peter S. Nelson
Division of Human Biology
Fred Hutchinson Cancer Research Center
Mailstop D4-100
1100 Fairview Ave N
Seattle, WA 98109-1024
Email: pnelson@fredhutch.org
Telephone: 206-667-3377

ABSTRACT

Purpose: Small-cell neuroendocrine prostate cancer (SCNPC) exhibits an aggressive clinical course and incidence rates appear to be increasing following resistance to potent androgen receptor (AR) antagonists. Currently, treatment options are limited and few model systems are available to identify new approaches for treatment. We sought to evaluate commonalities between SCNPC and other aggressive neuroendocrine carcinomas to identify therapeutic targets.

Experimental Design: We generated whole transcriptome RNAseq data from AR-active prostate cancers (ARPC) and SCNPCs from tumors collected at rapid autopsy, and two other NE carcinomas, Merkel Cell Carcinoma (MCC) and small-cell lung cancer (SCLC). We performed cross-tumor comparisons to identify conserved patterns of expression of druggable targets. We tested inhibitors to highly upregulated drug targets in a panel of PC cell lines and *in vivo* patient-derived xenograft (PDX) models.

Results: We identified BCL2 as highly upregulated in SCNPC compared to ARPC. Inhibitors targeting BCL2 induced apoptotic cell death in SCNPC cell lines at nanomolar concentrations while ARPC cell lines were resistant. Treatment with the BCL2 inhibitor Navitoclax lead to a reduction of growth of SCNPC PDX tumors *in vivo*, while ARPC PDX models were more resistant. We identified Wee1 as a second druggable target upregulated in SCNPC. Treatment with the combination of Navitoclax and the Wee1 inhibitor AZD-1775 repressed the growth of SCNPC PDX resistant to single agent BCL2 inhibitors.

Conclusions: The combination of BCL2 and Wee1 inhibition presents a novel therapeutic strategy for the treatment of SCNPC.

Statement of Translational Relevance: BCL2 inhibition may have single-agent efficacy in subsets of SCNPC. The efficacy of the dual inhibition of BCL2 and Wee1 in pre-clinical models represents a therapeutic strategy with the potential to overcome resistance to BCL2 inhibitors.

INTRODUCTION

Prostate cancer (PC) is notable for a general dependency on androgen receptor (AR) signaling for survival and proliferation, a feature which has served as the major focal point of treating metastatic PC for decades. However, a small subset of PCs exhibit histologic characteristics of small cell carcinomas similar to small cell cancers found in other organs with small-blue-round-cell morphology and the expression of proteins associated with neuroendocrine (NE) functions such as chromogranin and synaptophysin (1). These carcinomas lack AR activity and respond poorly to AR-directed therapy. While *de novo* small cell PC is very rare representing <1% of all PCs at diagnosis (2), in the context of intense therapeutic pressures designed to antagonize AR signaling, a subset of resistant PCs lose or attenuate the expression of AR regulated genes and gain the expression of NE-associated genes without exhibiting small cell morphology. These PCs which we collectively refer to as small-cell or neuroendocrine prostate cancer (SCNPC) respond poorly to conventional therapies and have substantially worse outcomes. Overt small cell PCs and the treatment-associated SCNPCs frequently demonstrate bi-allelic inactivation of *RB1* and *TP53* tumor suppressor genes. Of interest, treatment-associated SCNPC often carry genomic alterations identical to the original adenocarcinoma, such as the *TMPRSS2-ERG* gene rearrangement, indicating either a common progenitor, or that SCNPC arises from the transdifferentiation of an existing adenocarcinoma following repression of the major lineage-directing AR program. Transdifferentiation has been described in other malignancies such as lung adenocarcinoma where resistance to EGFR inhibition is associated with the emergence of small cell lung cancer (SCLC) phenotypes (3,4). The molecular events regulating transdifferentiation and the acquisition of NE characteristics is an active area of investigation.

The aggressive behavior of SCNPC underscores a critical need in the field to identify effective therapeutic strategies. One approach, centered on defining the major differences in oncogenic drivers between AR-active PCs and those with SCNPC characteristics, identified MYCN (5,6), an oncogene implicated in the initiation of other NE tumor types such as neuroblastoma and whose expression and/or amplification is also associated with SCLC (7-9). A common mechanism has been proposed by which Aurora kinase A stabilizes N-Myc protein in both MYCN-amplified neuroblastoma and MYCN-amplified SCNPC (5,10). Clinical trials with the Aurora kinase inhibitor Alisertib have demonstrated that a subset of patients with molecular features supporting Aurora-A and N-Myc activation exhibited significant clinical benefit (11).

To date, most studies of SCNPC have focused on comparing tumors of prostate origin. However, the rarity of SCNPC and lack of model systems with which to interrogate the disease and test potential therapeutics has constrained progress. Recent ‘pan-cancer’ analyses indicate that comparisons of cancer subtypes arising in divergent organ sites can yield information with respect to cell of origin, common developmental processes, and actionable targets. Notably, a pan-cancer analysis identified

an adult stem cell signature that associates with aggressive variants across epithelial neoplasms and which was particularly elevated in small cell/neuroendocrine tumors (12).

In this study our objective was to identify therapeutic vulnerabilities in SCNPCs. To ascertain potential targets, we evaluated the transcriptional programs of three tumor types that exhibit small cell and/or NE features: SCNPC, SCLC, and Merkel cell carcinoma (MCC). Focusing on the druggable genome, we identified several candidates including BCL2 and Wee1, and demonstrated preclinical *in vitro* and *in vivo* efficacy of clinical inhibitors against BCL2 and Wee1. These studies provide rationale to evaluate the efficacy of BCL2 and Wee1 directed therapy in patients with SCNPC.

METHODS AND MATERIALS

Patient sample and RNA collection. Prostate cancer metastases were collected as part of the Prostate Cancer Donor Program at the University of Washington. Collection of samples and RNA isolation of UW prostate cancer samples was carried out as previously described (13). Merkel cell carcinoma patient samples and RNA were collected as part of a previously published study (14). SCLC patient samples were obtained through the Cooperative Human Tissue Network. SCLC cell lines NCI-H1436, NCI-H1672, NCI-H1963, NCI-H2141, NCI-H2195, NCI-H735, NCI-H774 were obtained from ATCC. RNA from tumor samples and cell lines was extracted with TRIzol (Invitrogen).

RNA-sequencing library prep and read processing. The purity and concentration of RNA was assessed by Nanodrop (Thermo Fisher) and Agilent Bioanalyzer. One microgram of total RNA was used as input to either the Illumina Tru Seq RNA Library Kit v2 or the Illumina TruSeq Stranded mRNA Library prep kit and libraries were prepared and barcoded according to the manufacturer's protocol. Libraries were sequenced on the Illumina HiSeq 2500 generating either 50 or 75 base-pair paired end reads. Resulting reads were mapped to the hg38 human genome with TopHat v2.0.14 and transcript abundance was measured using the R Bioconductor package Genomic Alignments v1.18.0. Sequencing reads from patient-derived xenograft libraries were aligned to both hg38 human and mm10 mouse genomes.

Statistical Analyses. Differential expression analyses of RNA-sequencing data were carried out using the Bioconductor package edgeR v3.24.2 with transcript abundances as input. An FDR threshold of <0.05 was used as a cut-off for differential expression assessment. Multi-dimensional scaling analysis was conducted with all measured genes as input to the R Bioconductor package limma v3.38.3.

Calculation of AR and NE signature scores were carried out using the Bioconductor package GSVA v1.30.0 using z-score normalized $\log_2$ FPKM values as input. Scatterplots were created using

ggplot2 v3.1.0 and the Pearson correlation between gene and signature score was calculated using the ggpubr v0.2 stat.cor() function.

Boxplots for individual genes were created with ggplot2 v3.1.0 and statistical assessment between groups was assessed by Student's t-test using the ggpubr v0.2 stat_compare_means() function.

Guilt-by-association analysis was performed by calculating the Pearson correlation between the log_2FPKM expression of the lncRNA with that of each protein coding gene across all samples. Absolute values of the Pearson correlations were sorted and the top 1% most highly correlated protein coding genes was used as input to identify enriched KEGG pathways with the gProfiler R package. Additional KEGG enrichment analysis was also performed with the gProfiler R package.

RNA-seq data from previously published datasets Bluemn et al., 2017, Aggarwal et al., 2018, and Abida et al. 2019 was analyzed and sample phenotypic groups were assigned for each cohort using classical multidimensional scaling (MDS) calculated with the cmdscale function in R on the expression profiles of 34 genes from the combined lists of "NEURO I", "NEURO II", and "AR" gene signatures in Labrecque et al (15) and the "NE" and "AR" signatures in Bluemn et al. (13). The distance metric was "euclidean" calculated by dist function on the columns (samples.)

Cell Lines. The cell lines, LNCaP (ATCC), C4-2 (ATCC), MSKCC EF1 (gift from John K. Lee), MKL-1 (Sigma), VCaP (ATCC), LAPC4 (gift of Charles Sawyers), NCI-H660 (ATCC), NCI-H82 and NCI-H69 (ATCC), MS-1 (Sigma) were maintained in a 37ºC incubator with 5% CO_2 and grown in medium supplemented with fetal bovine serum and other additives as recommended by ATCC or the cell line provider. STR genotyping was used to authenticate the lines and cells were confirmed to be mycoplasma free using the MycoAlert Detection Kit (Lonza, LT07-418). Cells were cultured no longer than 10 passages after thawing and before experimental use.

Protein isolation and immunoblotting. Cell lines were washed 1x with PBS prior to the addition of a cell lysis buffer (1.5M Urea, 1% SDS, 1% NP-40, 2% Tween20, 250 nM NaCl, PBS) supplemented with 1x phosphatase inhibitors (PhosStop, Roche Diagnostics) and a 1x protease inhibitor cocktail (Complete Mini, Roche Diagnostics). PDX tissues were pulverized in liquid nitrogen with a mortar and pestle prior to the addition of lysis buffer. Lysates were sonicated and then centrifuged to clear debris. Protein quantification was performed using the Pierce bicinchoninic acid assay (Thermo Scientific). Lysates were run on a 4-12% NuPage Bis-Tris gel and protein was transferred to a nitrocellulose membrane in Tris/CAPS buffer using a semi-dry transfer apparatus. Membranes were blocked and incubated with antibody solutions in 5% milk powder in 1x PBS with 0.01% Tween. Primary antibodies targeting BCL2 (Santa Cruz Biotechnologies, sc-7382, 1:500), BCL-XL (Cell Signaling, 2764, 1:1000), BCLW (Cell Signaling, 2724, 1:1000), Cleaved Caspase-3 (Cell Signaling, 9661S, 1:1000), WEE1 (Cell Signaling, 13084, 1:1000) phospho-cdc2(Tyr15) (Cell Signaling, 4539, 1:1000), AR

(Abcam, ab133273, 1:2000), PSA (Santa Cruz Biotechnologies, sc7638, 1:100) and GAPDH (Bio-Rad, hFAB Rhodamine, cat# 12004167, 1:5000) were used. Secondary antibodies used were Goat-anti-Rabbit (Goat anti-Rabbit IgG (H+L) Secondary Antibody, HRP cat# 31460, 1:5000) and Goat-anti-Mouse (BioRad, StarBright Blue 700 cat# 12004158, 1:5000). Blots were imaged using the Chemi-Doc MP (BioRad).

Immunohistochemistry. LuCaP tissue microarrays (TMAs) were constructed and stained as previously described (16). Antibodies directed toward the detection of BCL2 [EPR17509] (Abcam, cat# ab182858) p-CDK1 (Abcam, ab-133463) and Wee1 (Santa Cruz Biotechnologies, sc-5258) were used according to the manufacturer's instructions. Staining assessment was blinded and the H-score was calculated and averaged across multiple tissue/tumor cores for the same LuCaP PDX line.

Drug treatments of cell lines. Cell lines were seeded in 96-well plates in 50µl media 24 hours before the addition of the inhibitor. Serial dilutions of inhibitors were made in media and 50ul of a 2x inhibitor solution were added to plates containing cells. At least three technical replicates for each dose were plated. The maximal amount of DMSO for each serial dilution was used as a vehicle control for all dose points. Viability was assessed 96 hours after addition of inhibitor using the Cell Titer-Glo 2.0 Assay (Promega), following the manufacturer's protocol. Dose-response curves shown are an average and standard deviation of 3 biological replicates for each cell line and each inhibitor. Non-linear regression curves were fitted to the average of biological replicates in GraphPad Prism7. Inhibitors used were ABT-199 (Selleckchem, S8048), ABT-263 (Selleckchem, S1001), Gambogic Acid (Selleckchem, S2448), A-1155463 (Selleckchem, S7800), and AZD-1775 (Selleckchem, S1525).

For assessment of cell death with cleaved caspase-3 immunoblot, cells were plated in 10cm dishes in media. After 24 hours, the media was changed to media containing DMSO or 100nM ABT-263. Cells were harvested 24 hours post-addition of drug and lysates collected as described.

Tumor Dissociation and Drug Treatment. LuCaP PDX tumors were harvested, minced, and placed in digestion media containing 1 mg/mL collagenase and 1 mg/mL dispase. Then, tumor mixtures were incubated at 37 degrees Celsius for 1 hour. Digested tissue was passed through 20G needles and 100m and 40m filters before counting. Cells were plated in 6-well dishes and treated with either vehicle (DMSO), AZD-1775 (500 nM final concentration), ABT-263 (final 10nM) or the combination AZD-1775 and ABT-263 (500nM + 10nM). After 72 hours, protein was harvested.

siRNA treatment of cell lines. Cells were plated 24 hours before transfection in 6-well or 96-well plates. Cells were transfected with 60nM (final concentration) Non-targeting siRNA (Dharmacon, cat # D-001206-13-20, siGENOME Non-Targeting siRNA Pool #1) or BCL2 siRNA (Dharmacon, cat# M-

003307-06-0010, SMARTpool: SiGENOME BCL2 siRNA) using TransIT-TKO Transfection Reagent (Mirus, cat# MIR 2154) following the manufacturer's instructions. Protein was collected and viability was assessed 96 hours post transfection. Data shown are an average and standard deviation of three biological replicates.

Patient derived xenograft studies. All animal procedures were approved by UW Institutional Animal Care and Use Committee (IACUC) and according to NIH guidelines. Male mice (n=24 per PDX) were implanted subcutaneously with tumor bits using a trocar. We used LuCaP 49, LuCaP 93, LuCaP 173.1, LuCaP 145.1, and LuCaP 145.2 SCNPC PDX models. When tumors reached ~100 mg, animals were randomized to treatment groups. We were aiming for three animals with tumor per arm: 1) control, 2) ABT-263; 3) AZD-1775, 4) ABT-263+AZD-1775. ABT-263 was formulated at 50/mg/kg in 10% ethanol, 30% polyethylene glycol 400 and 60% Phosal 50PG and AZD1775 was formulated at 60mg/kg in 0.5% w/v methyl cellulose. Both drugs were administered by oral gavage once a day, with five days on-two days off regimen. In the combination group ABT-263 was administered first and AZD-1775 90 minutes later. Treatments were administered for four weeks. Tumor volume and body weight were measured twice a week. Animals were sacrificed at four weeks, when tumors exceed 1000mg or when animal health was compromised.

RESULTS

Neuroendocrine carcinomas from different tissues of origin share gene expression programs.

To identify potential therapeutic targets in SCNPC, we began by defining transcriptional programs associated with NE carcinomas across tissue types. We evaluated whole-transcriptome RNA-sequencing (RNAseq) data that included 25 PC metastases from a previously published study (17), and newly generated RNAseq data from 91 castration-resistant prostate cancer (CRPC) metastases, 8 MCC patient tumors and 12 SCLC metastases or cell lines. We first sub-classified the CRPC tumors using a published 10 gene signature of AR program activity and a 10 gene signature associated with NE differentiation (13) (**Fig. 1A**). We designated AR+/NE- tumors as AR program-active prostate cancers (ARPCs), and AR-/NE+ tumors as small cell/neuroendocrine prostate cancers (SCNPCs). MCC and SCLC exhibited high expression of NE-signature genes in concordance with samples in the SCNPC category, and did not express AR-signature genes (**Fig. 1A**). On a global level, multi-dimensional scaling analysis demonstrated that MCC and SCLC cluster with SCNPC samples and away from ARPCs (**Fig. 1B**). We next sought to identify additional genes that distinguish SCNPC from ARPCs and found 817 genes with high consistent differential expression (|logFC |≥4 and FDR<0.05)

that also displayed similar expression across MCC and SCLC (**Fig. 1C**). Disregarding the level of differential expression, 4,988 out of 20,413 genes measured by RNA-sequencing distinguished ARPC from NE-associated cancers (FDR<0.05). The genes commonly upregulated in the NE-associated cancers are enriched for KEGG pathways associated with neuronal and cell cycle-related pathways (**Fig. S1A**).

The gene expression programs associated with NE differentiation comprise both unique effector proteins that carry out specialized cell functions as well as transcription factors that regulate the activity of downstream networks dictating cell identity. We next sought to determine which shared transcription factors (TFs) across NE tumors may drive a common cell fate and potentially regulate shared therapeutic targets. To meet the criteria of a TF, we combined human TFs from the Functional Anno-Tation Of the Mammalian Genome (FANTOM5) database with all proteins that were associated with "transcription factor activity" in the AmiGO database. Of the 4,988 conserved NE-associated genes, 444 met the TF criteria. Notably, the most-highly expressed TFs include several known to regulate neuronal or NE differentiation programs, including SOX2, NEUROD1, and HES6 (**Fig. 1D**). The most differentially upregulated TF between ARPCs and NE tumors, ST18, is associated with neuronal differentiation and is highly expressed in endocrine cells in the pancreas. Another highly upregulated transcription factor, MYT1L, has been implicated in the maintenance of NE differentiation (18), and can reprogram fibroblasts into neurons when co-expressed with BRN2 and ASCL1 (19). Elevated MYT1L is correlated with poor prognosis in patients with medulloblastoma (20), another small cell tumor type.

Members of the MYC family of transcription factors are commonly altered in PC. Consistent with previous findings, MYC is expressed highly in ARPCs (**Fig. 1E**) whereas MYCN is elevated in all three NE tumor types profiled relative to ARPC (**Fig. 1F**). We found that MYCL is also highly expressed across the three NE tumor types relative to ARPC (**Fig. 1G**), and has recently been implicated in the initiation of SCLC (21).

Long non-coding RNAs (lncRNAs) are typically lowly expressed but are highly tissue specific. The expression of lncRNAs has been associated with prognosis in some cancers, including small-cell NE cancers. Several lncRNAs, such as HOTAIR and Schlap-1 are associated with PC proliferation and invasion (22,23). We derived a list of lncRNAs and pseudogenes from ENSEMBL and NCBI GRch38 annotations and determined that 447 out of 2283 lncRNAs and pseudogenes quantitated by RNA-sequencing are upregulated across SCNPC, SCLC and MCC relative to ARPCs (**Fig. S1B**). As the majority of lncRNAs have unknown functions, we conducted a guilt-by-association analysis for the top 50 most highly expressed NE-associated lncRNAs (24). These 50 lncRNAs have high correlation to protein coding genes associated with KEGG pathways related to neuronal processes and PC (**Fig. S1C**).

Recent studies profiling the temporal alterations in gene expression during transitions from ARPC to SCNPC identified several hundred lncRNAs associated with the acquisition of the SCNPC phenotype (25). Notably, the expression of several lncRNAs is associated with the rapid development of metastasis following ADT. We found a high degree of overlap between the lncRNAs upregulated across the NE cancers we evaluated, and those explicitly associated with PC transdifferentiation: of 122 transcripts comprising a lncRNA SCNPC signature, 100 (80%; $p<0.0001$) were differentially regulated across SCLC and MCC. Although lncRNAs may serve as markers of NE differentiation and have utility in predicting treatment outcomes, they are currently challenging to exploit as therapeutic targets.

Profiling the druggable genome across NE tumors identifies therapeutic targets in SCNPC

To identify potential conserved dependencies on druggable targets amongst NE tumors, we profiled the expression of genes comprising the druggable genome (26). Of 4,026 druggable targets measured, 875 had similar expression across NE tumors relative to ARPCs (**Fig. 2A**). A subset of druggable targets are represented by cell surface proteins expressed uniquely on subtypes of neoplastic cells that can be exploited for immune-based therapy and for antibody or small molecule delivery of targeted therapeutics. Notably, the Notch ligand receptor DLL3 was among the top differentially upregulated cell surface proteins between ARPCs and the NE tumors (**Fig. 2A,B**). DLL3 has previously been shown to be upregulated in SCLC. An antibody-drug conjugate, Rovalpituzumab tesirine, has demonstrated clinical efficacy toward SCLCs and is currently being investigated in clinical trials (27). As with the human tumors, we found that DLL3 expression was upregulated in NEPC PDX models compared to ARPC PDX models (**Fig. 2C**). These data suggest that therapeutics targeting DLL3 may be broadly effective across NE tumors including SCLC, SCNPC and MCC.

Additional targets that exhibited differential upregulation in NE tumors relative to ARPCs include aurora kinase A and B (AURKA, AURKB), the anaplastic lymphoma kinase A (ALK), and the bromodomain and extra terminal domain family member BRD4 (**Fig. 2A**). Recent studies have demonstrated the efficacy of BET inhibitor therapy in preclinical models of SCLC with downregulation of the neuronal lineage transcription factor ASCL1 and the induction of apoptosis (28). Further, BET inhibitors have been shown in preclinical studies to be particularly effective in MYC-driven cancers such as neuroblastoma (29), which is also a feature of SCNPCs where MYCN and MYCL are highly expressed.

BCL2 is a therapeutic target in SCNPC

Transcripts encoding the antiapoptotic protein BCL2 were among the most highly expressed druggable targets across NE carcinomas (**Fig. 2A,D**). We chose to focus on BCL2 as both MCC and subsets of SCLC have previously been shown to be sensitive to BCL2 family inhibitors but their effects have not been described in SCNPC (30,31). We determined that other frequently co-targeted members of the BCL2 family, BCLXL and BCLW were not differentially upregulated in SCNPC (**Fig.**

S2A,B). BCL2 expression was significantly higher in SCNPCs versus ARPCs in 3 independent studies of metastatic CRPC (**Fig. 2E-G**)(13,32,33). BCL2 expression is also significantly positively correlated with the 10 gene NE-signature score and significantly negatively correlated with AR-activity (**Fig. 2H,I**). BCLXL expression has no significant correlation with either signature score and BCLW expression is positively correlated with AR-activity and negatively correlated with the NE-signature (**Fig. S2C-F**).

We next assayed BCL2 family protein levels across a panel of cell lines that include ARPC, represented by LNCaP, C4-2, LAPC4 and VCaP, and SCNPC, represented by the NCI-H660 and MSKCC EF1 lines. MCC lines are designed MKL-1 and MS-1. SCLC lines are NCI-H69, NCI-H82. In agreement with the tumor-derived transcript data, BCL2 protein is highly expressed across the majority of the NE cell lines, including NCI-H660, and was not detectable in the ARPC lines (**Fig. 2J**).

We next assessed the responses to pharmacological inhibitors of BCL2 family proteins across ARPC and SCNPC cells. We determined that SCNPC NCI-H660 and MSKCC EF1 cells are substantially more sensitive to the pan BCL-XL, BCL-W, and BCL2 inhibitor ABT-263, and the more selective BCL2 inhibitor, ABT-199, than other prostate lines profiled (**Fig. 3A,B**). For example, the approximate IC50 concentrations of ABT-199/Venetoclax in NCI-H660 versus the ARPC LNCaP are 50nM vs 500nM, respectively. In addition, NCI-H660 and MSKCC EF1 have comparable sensitivity to other prostate lines when treated with the more selective BCL-XL inhibitor A115463 (**Fig. 3C**) or the more selective BCL-W inhibitor, Gambogic Acid (**Fig. 3D**). A 24 hour treatment with 100nM ABT-263 is sufficient to induce cell death in NCI-H660 SCNPC cells, as evidenced by cleaved caspase-3 whereas ARPCs showed no evidence of an apoptotic response (**Fig. 3E**). We also profiled the response of this prostate cancer cell line panel to older generation BCL2 inhibitors Sabutoclax, Obatoclax, and a selective MCL1 inhibitor, A1210477. However NCI-H660 was equally or less sensitive to these compounds than other prostate cancer cell lines (**Fig. S3A-D**). In agreement with the pharmacological studies, siRNA knockdown of BCL2 decreased viability of NCI-H660 but not LNCaP cells (**Fig. S3E-H**).

To further assess the efficacy and specificity of targeting BCL2 in SCNPC, we evaluated the effects of pharmacological BCL2 inhibition on patient derived xenograft (PDX) models of SCNPC. RNA-seq confirmed that SCNPC PDX tumors expressed significantly higher levels of BCL2 transcripts compared to ARPC PDX tumors (**Fig 3F**). These findings were confirmed by Western Blot analysis of BCL2 protein in on a panel of PC PDX tumors: BCL2 protein was highly expressed in five of five SCNPC PDX lines whereas 3 of 4 ARPC PDX lines had no detectable BCL2 and 1 expressed low levels (**Fig 3G**). Immunohistochemical analysis confirmed high BCL2 expression in SCNPC relative to ARPC tumors with the majority of ARPCs having no detectable staining (**Fig. 3H**). Mirroring the patient tumors, BCL2 expression levels in PDX models are positively correlated with the NE-signature score (**Fig. 3I**).

We treated 5 castration-resistant SCNPC PDX models, LuCaP49, LuCaP93, LuCaP173.1, LuCaP145.1, and LuCaP145.2 with the BLC2 antagonist ABT-263/Navitoclax. Compared to vehicle control, ABT-263 significantly reduced the growth of 2 lines, LuCaP49 and LuCaP173.1 for an overall response rate of 40% (**Fig. 3J**). Notably, LuCaP49 PDX tumor volumes at the 4-week end of study evaluation were over 4 times smaller for ABT-263 treatment than vehicle control (p =0.05 by Student's t-test).

Targeting the Wee1 Kinase with BCL2 inhibition represses SCNPC growth

While the *in vitro* studies indicated that NE carcinomas cells are sensitive to BCL2 antagonism and two *in vivo* PDX models of SCNPC confirmed the anti-tumor activity of BCL2 inhibition, we determined that three SCNPC PDX lines were resistant to ABT-263 (**Fig. 3J**). BCL2 levels in the resistant PDX tumors approximated the levels of BCL2 in the responsive tumors (**Fig. 3G**). We evaluated protein levels of other BCL2 family members that may contribute to resistance to ABT-263 in the PDX tumors, however no single protein was able to distinguish responding vs. non-responding models **(Fig. S3I)**. We next evaluated the druggable genome data for additional differentially expressed targets with available pharmacological inhibitors. These analyses determined that the mitotic checkpoint kinase Wee1 is differentially upregulated in NE carcinomas versus ARPCs (**Fig. 4A-D**). Wee1 expression was negatively associated with AR activity in PC metastases and PDX lines and positively associated with NE activity in PC PDX models (**Fig. 4E-I**). We confirmed that Wee1 protein is highly expressed in SCNPC cell lines and PDX models compared to ARPC models, as assessed by Western Blot and IHC (**Fig. 4J,K and S4A,B**). Notably, Wee1 inhibition has demonstrated efficacy in neuroblastoma, small cell lung cancer, medulloblastoma, and other NE-associated malignancies (34-38).

We evaluated the effects of the Wee1 antagonist AZD-1775 across the SCNPC PDX models and SCNPC cell lines. As a single agent, AZD-1775 has minimal activity toward SCNPC cell lines in vitro, though more substantial effects toward ARPC lines (**Fig. S5A-D**). We next combined AZD-1775 with ABT-263. These drugs exhibited synergy in the SCNPC lines with a combination index score of 0.556 in NCI-H660 (**Fig. S5E,F**) while demonstrating at best additive effects in the ARPC lines tested (**Fig. S5G,H**). To assess on-target Wee1 inhibition, we measured the phosphorylation of downstream kinase CDK1 and confirmed that exposure to AZD-1775 reduced the inhibitory phosphorylation of this key regulator of mitosis (**Fig S4C-E**). Consistent with the in vitro results, only very modest single agent AZD-1775 activity was observed in 2 SCNPC PDX models with 3 showing no responses (**Fig. 4N**). The combination of ABT-263 and AZD-1775 significantly inhibited the growth of four of five SCNPC PDX lines (80% response rate). Notably, the ABT-263-resistant LuCaP93 SCNPC line demonstrated marked sensitivity to the drug combination with average end of study tumor volumes 4 times larger in control or AZD-1775 treatment arms versus AZD-1775 plus ABT-263 (**Fig. 4N**) (p=0.017, Student's t-test).

DISCUSSION

The emergence of therapy-associated neuroendocrine differentiation in patients with metastatic prostate cancer portends a short survival with very limited benefit from current therapeutics. These poor outcomes are mirrored by low survival rates in other neuroendocrine tumors such as small cell lung cancer and metastatic Merkel cell carcinoma. Notably, these malignancies share a number of oncogenic features that include loss of TP53 and RB1 tumor suppressor function and gain of MYC activity. In the present study we identified additional phenotypic similarities that include a large number of co-expressed lncRNAs, transcription factors that influence neuronal and neuroendocrine activity, and cell surface proteins that represent viable therapeutic targets. As the majority of SCNPCs included in the present study were associated with treatment, future studies are required to confirm concordance with *de novo* SCPC.

MYCN is perhaps the most notable transcription factor proposed to drive neuroendocrine cancers arising in diverse organs including neuroblastoma, SCLC and SCNPC where it may function to promote lineage switching (39,40). We found that MYCL, another MYC family member recently implicated in the initiation of SCLC (21), is also highly expressed in MCC and SCNPC. In addition, we identified 373 transcription factors with expression patterns conserved across MCC, SCLC, and SCNPC. Whether these factors are driving the neuroendocrine phenotype or are merely a consequence of it, remains to be explored.

LncRNAs represent a class of transcripts attracting attention for their roles in promoting the malignant features of some tumors. We identified 285 lncRNAs with conserved expression patterns across MCC, SCLC, and NEPC. Of the most highly expressed pan neuroendocrine-associated lncRNAs we identified, MIAT and LINC01346 have high correlation with the expression of genes involved in the KEGG prostate cancer pathway. MIAT has previously been identified as highly expressed in NEPC, however LINC01346 has no previously described connection to prostate cancer. The elevated expression of MIAT and LINC01346 and their pan-neuroendocrine correlation suggest that it may also play a role in supporting the growth or maintenance of these tumors.

The identification of cancer-specific cell surface molecules is increasingly relevant with the advent of successful Chimeric Antigen Receptor (CAR) T-cell therapies and antibody-drug conjugates (ADCs). ADCs directed toward the cell surface protein DLL3 have produced responses in patients with SCLC and SCNPC (27,41). CEACAM5 was recently identified as a cell surface antigen selectively enriched in SCNPC (42). Although CEACAM5 is highly expressed in SCNPC and SCLC, we found it to be lowly expressed in MCC and therefore did not fall into our list of pan neuroendocrine-associated genes.

We identified several potential druggable targets spanning SCNPC, SCLC, and MCC that included the anti-apoptotic protein BCL2. Elevated BCL2 protein expression has been identified in multiple neuroendocrine tumor types, though not specifically SCNPC, and BCL2 inhibition has recently been shown to induce cell death in MCC and SCLC cell lines with high levels of BCL2 protein (30,31). A generalized model to explain high levels of anti-apoptotic BCL2 family member expression in many cancers has been proposed in which a cell undergoing oncogenic transformation will be subjected to higher apoptotic-stress and upregulation of pro-apoptotic BCL2 family members; thus the cell needs to acquire compensatory alterations to overcome apoptotic cues. In lymphomas, MYC amplifications are often seen in conjunction with BCL2 amplification and in neuroblastoma, MYCN amplification is correlated with higher BCL2 levels (43). In prostate cancer, the AR has been shown to directly repress BCL2 transcription and consequently AR antagonist therapy results in elevated BCL2 (44,45).

Though BCL2 has long been viewed as an attractive therapeutic target, only recently have inhibitors been developed with potent anti-BCL2 activity and tolerable side-effect profiles. The BCL-2 antagonist Venetoclax was recently approved as a treatment for chronic lymphocytic leukemia and acute myelogenous leukemia, and clinical trials in other tumor types are underway. Recent studies demonstrated effects of BCL2 inhibition in preclinical models of AR-low prostate cancers and in combination with AR blockade in AR-active preclinical models (45). Although the combination of BCL2 and Wee1 inhibition is novel, it has previously been proposed that BCL2 family proteins can regulate sensitivity to anti-mitotic agents (46,47). CDK1, negatively regulated by Wee1, phosphorylates and inactivates anti-apoptotic BCL2 family members, including BCL2, during prolonged mitosis leading to cell death (48,49). It is our hypothesis that further inhibition of BCL2 results in the synergistic effects of AZD-1775 and ABT-263. Our studies support testing BCL2 inhibitors in patients with AR-null SCNPC, and evaluating additional therapeutics such as Wee1 antagonists that could synergize with BCL2-directed therapeutics in SCNPCs that resist single-agent treatment.

DISCLOSURE OF POTENTIAL CONFLICTS OF INTEREST

PSN is a paid consultant/advisor to Janssen and Astellas.

AUTHORS CONTRIBUTIONS

A.N.C., D.M., P.N., E.C., and P.S.N. designed the research; A.N.C., M.V.A.C.O, J.M.L., I.C., A.K., H.M.N., D.S., L.G.B., L.T., C.M., and E.C., performed the research; A.N.C., E.C., R.G., I.C., and P.S.N. analyzed the data; A.N.C., and P.S.N. wrote the paper and all authors edited and approved the final manuscript.

ACKNOWLEDGEMENTS

We are grateful to the patients who participated in these studies. We thank Abbvie for providing ABT-263 and AstraZeneca for providing AZD-1775 for these studies. We thank the FredHutch Genomics and Bioinformatics and Comparative Medicine shared resources for assistance and expertise. We thank members of the Nelson laboratory for constructive suggestions. We gratefully acknowledge research support from the Prostate Cancer Foundation and Kelsey Dickson Challenge Award (P.Nghiem, P.Nelson). This research was also supported by Cancer Center Support Grant P30CA015704-40 (P.Nelson, J.Lee, D.MacPherson), P50CA097186-14S1 (P.Nelson, E.Corey, H.Nguyen, D.Sondheim, L.Brown, R.Gulati, L.True), U54CA224079 (E.Corey, P.Nelson, I.Coleman) and Department of Defense grants W81XWH17-1-0415 (C.Morrissey, P.Nelson, A.Corella, M.Ordonio) and W81XWH-18-1-0347 (P.Nelson, J.Lucas). ANC was supported by the NIH Chromosome Metabolism Training Grant 2T32CA009657 and the Ford Dissertation Fellowship administered by the National Academies of Sciences, Engineering, and Medicine.

REFERENCES

1. Rajwanshi A, Srinivas R, Upasana G. Malignant small round cell tumors. J Cytol **2009**;26(1):1-10 doi 10.4103/0970-9371.54861.
2. Nadal R, Schweizer M, Kryvenko ON, Epstein JI, Eisenberger MA. Small cell carcinoma of the prostate. Nature reviews Urology **2014**;11(4):213-9 doi 10.1038/nrurol.2014.21.
3. Niederst MJ, Sequist LV, Poirier JT, Mermel CH, Lockerman EL, Garcia AR*, et al.* RB loss in resistant EGFR mutant lung adenocarcinomas that transform to small-cell lung cancer. Nat Commun **2015**;6:6377 doi 10.1038/ncomms7377.
4. Oser MG, Niederst MJ, Sequist LV, Engelman JA. Transformation from non-small-cell lung cancer to small-cell lung cancer: molecular drivers and cells of origin. Lancet Oncol **2015**;16(4):e165-72 doi 10.1016/S1470-2045(14)71180-5.
5. Beltran H, Rickman DS, Park K, Chae SS, Sboner A, MacDonald TY*, et al.* Molecular characterization of neuroendocrine prostate cancer and identification of new drug targets. Cancer Discov **2011**;1(6):487-95 doi 10.1158/2159-8290.CD-11-0130.
6. Lee JK, Phillips JW, Smith BA, Park JW, Stoyanova T, McCaffrey EF*, et al.* N-Myc Drives Neuroendocrine Prostate Cancer Initiated from Human Prostate Epithelial Cells. Cancer Cell **2016**;29(4):536-47 doi 10.1016/j.ccell.2016.03.001.
7. George J, Lim JS, Jang SJ, Cun Y, Ozretic L, Kong G*, et al.* Comprehensive genomic profiles of small cell lung cancer. Nature **2015**;524(7563):47-53 doi 10.1038/nature14664.
8. Peifer M, Fernandez-Cuesta L, Sos ML, George J, Seidel D, Kasper LH*, et al.* Integrative genome analyses identify key somatic driver mutations of small-cell lung cancer. Nat Genet **2012**;44(10):1104-10 doi 10.1038/ng.2396.
9. Rudin CM, Durinck S, Stawiski EW, Poirier JT, Modrusan Z, Shames DS*, et al.* Comprehensive genomic analysis identifies SOX2 as a frequently amplified gene in small-cell lung cancer. Nat Genet **2012**;44(10):1111-6 doi 10.1038/ng.2405.
10. Otto T, Horn S, Brockmann M, Eilers U, Schuttrumpf L, Popov N*, et al.* Stabilization of N-Myc is a critical function of Aurora A in human neuroblastoma. Cancer Cell **2009**;15(1):67-78 doi 10.1016/j.ccr.2008.12.005.
11. Beltran H, Oromendia C, Danila DC, Montgomery B, Hoimes C, Szmulewitz RZ*, et al.* A Phase II Trial of the Aurora Kinase A Inhibitor Alisertib for Patients with Castration-resistant and Neuroendocrine Prostate Cancer: Efficacy and Biomarkers. Clin Cancer Res **2019**;25(1):43-51 doi 10.1158/1078-0432.CCR-18-1912.
12. Smith BA, Balanis NG, Nanjundiah A, Sheu KM, Tsai BL, Zhang Q*, et al.* A Human Adult Stem Cell Signature Marks Aggressive Variants across Epithelial Cancers. Cell Rep **2018**;24(12):3353-66 e5 doi 10.1016/j.celrep.2018.08.062.

13. Bluemn EG, Coleman IM, Lucas JM, Coleman RT, Hernandez-Lopez S, Tharakan R*, et al.* Androgen Receptor Pathway-Independent Prostate Cancer Is Sustained through FGF Signaling. Cancer Cell **2017**;32(4):474-89 e6 doi 10.1016/j.ccell.2017.09.003.
14. Paulson KG, Iyer JG, Tegeder AR, Thibodeau R, Schelter J, Koba S*, et al.* Transcriptome-wide studies of merkel cell carcinoma and validation of intratumoral CD8+ lymphocyte invasion as an independent predictor of survival. J Clin Oncol **2011**;29(12):1539-46 doi 10.1200/JCO.2010.30.6308.
15. Labrecque MP, Coleman IM, Brown LG, True LD, Kollath L, Lakely B*, et al.* Molecular profiling stratifies diverse phenotypes of treatment-refractory metastatic castration-resistant prostate cancer. J Clin Invest **2019**;130 doi 10.1172/JCI128212.
16. Roudier MP, Winters BR, Coleman I, Lam HM, Zhang X, Coleman R*, et al.* Characterizing the molecular features of ERG-positive tumors in primary and castration resistant prostate cancer. Prostate **2016**;76(9):810-22 doi 10.1002/pros.23171.
17. Beltran H, Prandi D, Mosquera JM, Benelli M, Puca L, Cyrta J*, et al.* Divergent clonal evolution of castration-resistant neuroendocrine prostate cancer. Nat Med **2016**;22(3):298-305 doi 10.1038/nm.4045.
18. Mall M, Kareta MS, Chanda S, Ahlenius H, Perotti N, Zhou B*, et al.* Myt1l safeguards neuronal identity by actively repressing many non-neuronal fates. Nature **2017**;544(7649):245-9 doi 10.1038/nature21722.
19. Vierbuchen T, Ostermeier A, Pang ZP, Kokubu Y, Sudhof TC, Wernig M. Direct conversion of fibroblasts to functional neurons by defined factors. Nature **2010**;463(7284):1035-41 doi 10.1038/nature08797.
20. Lastowska M, Al-Afghani H, Al-Balool HH, Sheth H, Mercer E, Coxhead JM*, et al.* Identification of a neuronal transcription factor network involved in medulloblastoma development. Acta Neuropathol Commun **2013**;1:35 doi 10.1186/2051-5960-1-35.
21. Kim DW, Wu N, Kim YC, Cheng PF, Basom R, Kim D*, et al.* Genetic requirement for Mycl and efficacy of RNA Pol I inhibition in mouse models of small cell lung cancer. Genes Dev **2016**;30(11):1289-99 doi 10.1101/gad.279307.116.
22. Prensner JR, Iyer MK, Sahu A, Asangani IA, Cao Q, Patel L*, et al.* The long noncoding RNA SChLAP1 promotes aggressive prostate cancer and antagonizes the SWI/SNF complex. Nat Genet **2013**;45(11):1392-8 doi 10.1038/ng.2771.
23. Zhang A, Zhao JC, Kim J, Fong KW, Yang YA, Chakravarti D*, et al.* LncRNA HOTAIR Enhances the Androgen-Receptor-Mediated Transcriptional Program and Drives Castration-Resistant Prostate Cancer. Cell Rep **2015**;13(1):209-21 doi 10.1016/j.celrep.2015.08.069.

24. Bester AC, Lee JD, Chavez A, Lee YR, Nachmani D, Vora S*, et al.* An Integrated Genome-wide CRISPRa Approach to Functionalize lncRNAs in Drug Resistance. Cell **2018**;173(3):649-64 e20 doi 10.1016/j.cell.2018.03.052.
25. Ramnarine VR, Alshalalfa M, Mo F, Nabavi N, Erho N, Takhar M*, et al.* The long noncoding RNA landscape of neuroendocrine prostate cancer and its clinical implications. Gigascience **2018**;7(6) doi 10.1093/gigascience/giy050.
26. Finan C, Gaulton A, Kruger FA, Lumbers RT, Shah T, Engmann J*, et al.* The druggable genome and support for target identification and validation in drug development. Science translational medicine **2017**;9(383) doi 10.1126/scitranslmed.aag1166.
27. Rudin CM, Pietanza MC, Bauer TM, Ready N, Morgensztern D, Glisson BS*, et al.* Rovalpituzumab tesirine, a DLL3-targeted antibody-drug conjugate, in recurrent small-cell lung cancer: a first-in-human, first-in-class, open-label, phase 1 study. Lancet Oncol **2017**;18(1):42-51 doi 10.1016/S1470-2045(16)30565-4.
28. Lenhart R, Kirov S, Desilva H, Cao J, Lei M, Johnston K*, et al.* Sensitivity of Small Cell Lung Cancer to BET Inhibition Is Mediated by Regulation of ASCL1 Gene Expression. Mol Cancer Ther **2015**;14(10):2167-74 doi 10.1158/1535-7163.MCT-15-0037.
29. Puissant A, Frumm SM, Alexe G, Bassil CF, Qi J, Chanthery YH*, et al.* Targeting MYCN in neuroblastoma by BET bromodomain inhibition. Cancer Discov **2013**;3(3):308-23 doi 10.1158/2159-8290.CD-12-0418.
30. Lochmann TL, Floros KV, Naseri M, Powell KM, Cook W, March RJ*, et al.* Venetoclax Is Effective in Small-Cell Lung Cancers with High BCL-2 Expression. Clin Cancer Res **2018**;24(2):360-9 doi 10.1158/1078-0432.CCR-17-1606.
31. Verhaegen ME, Mangelberger D, Weick JW, Vozheiko TD, Harms PW, Nash KT*, et al.* Merkel cell carcinoma dependence on bcl-2 family members for survival. The Journal of investigative dermatology **2014**;134(8):2241-50 doi 10.1038/jid.2014.138.
32. Aggarwal R, Huang J, Alumkal JJ, Zhang L, Feng FY, Thomas GV*, et al.* Clinical and Genomic Characterization of Treatment-Emergent Small-Cell Neuroendocrine Prostate Cancer: A Multi-institutional Prospective Study. J Clin Oncol **2018**;36(24):2492-503 doi 10.1200/JCO.2017.77.6880.
33. Robinson D, Van Allen EM, Wu YM, Schultz N, Lonigro RJ, Mosquera JM*, et al.* Integrative clinical genomics of advanced prostate cancer. Cell **2015**;161(5):1215-28 doi 10.1016/j.cell.2015.05.001.
34. Bauer TM, Jones SF, Greenlees C, Cook C, Mugundu GM, Jewsbury PJ*, et al.* A phase Ib, open-label, multicenter study to assess the safety, tolerability, pharmacokinetics, and antitumor activity of AZD1775 monotherapy in patients with advanced solid tumors: initial findings. Cancer Research **2016**;76.

35. Guertin AD, Li J, Liu Y, Hurd MS, Schuller AG, Long B*, et al.* Preclinical evaluation of the WEE1 inhibitor MK-1775 as single-agent anticancer therapy. Mol Cancer Ther **2013**;12(8):1442-52 doi 10.1158/1535-7163.MCT-13-0025.
36. Hanmod SS, Wang G, Edwards H, Buck SA, Ge Y, Taub JW*, et al.* Targeting histone deacetylases (HDACs) and Wee1 for treating high-risk neuroblastoma. Pediatric blood & cancer **2015**;62(1):52-9 doi 10.1002/pbc.25232.
37. Matheson CJ, Venkataraman S, Amani V, Harris PS, Backos DS, Donson AM*, et al.* A WEE1 Inhibitor Analog of AZD1775 Maintains Synergy with Cisplatin and Demonstrates Reduced Single-Agent Cytotoxicity in Medulloblastoma Cells. ACS chemical biology **2016**;11(7):2066-7 doi 10.1021/acschembio.6b00466.
38. Zhang M, Dominguez D, Chen S, Fan J, Qin L, Long A*, et al.* WEE1 inhibition by MK1775 as a single-agent therapy inhibits ovarian cancer viability. Oncology letters **2017**;14(3):3580-6 doi 10.3892/ol.2017.6584.
39. Mosquera JM, Beltran H, Park K, MacDonald TY, Robinson BD, Tagawa ST*, et al.* Concurrent AURKA and MYCN gene amplifications are harbingers of lethal treatment-related neuroendocrine prostate cancer. Neoplasia **2013**;15(1):1-10.
40. Rickman DS, Schulte JH, Eilers M. The Expanding World of N-MYC-Driven Tumors. Cancer Discov **2018**;8(2):150-63 doi 10.1158/2159-8290.CD-17-0273.
41. Puca L, Gavyert K, Sailer V, Conteduca V, Dardenne E, Sigouros M*, et al.* Delta-like protein 3 expression and therapeutic targeting in neuroendocrine prostate cancer. Science translational medicine **2019**;11(484) doi 10.1126/scitranslmed.aav0891.
42. Lee JK, Bangayan NJ, Chai T, Smith BA, Pariva TE, Yun S*, et al.* Systemic surfaceome profiling identifies target antigens for immune-based therapy in subtypes of advanced prostate cancer. Proc Natl Acad Sci U S A **2018**;115(19):E4473-E82 doi 10.1073/pnas.1802354115.
43. Castle VP, Heidelberger KP, Bromberg J, Ou X, Dole M, Nunez G. Expression of the apoptosis-suppressing protein bcl-2, in neuroblastoma is associated with unfavorable histology and N-myc amplification. Am J Pathol **1993**;143(6):1543-50.
44. Bruckheimer EM, Spurgers K, Weigel NL, Logothetis C, McDonnell TJ. Regulation of Bcl-2 expression by dihydrotestosterone in hormone sensitive LNCaP-FGC prostate cancer cells. J Urol **2003**;169(4):1553-7 doi 10.1097/01.ju.0000055140.91204.c7.
45. Li Q, Deng Q, Chao HP, Liu X, Lu Y, Lin K*, et al.* Linking prostate cancer cell AR heterogeneity to distinct castration and enzalutamide responses. Nat Commun **2018**;9(1):3600 doi 10.1038/s41467-018-06067-7.
46. Inuzuka H, Shaik S, Onoyama I, Gao D, Tseng A, Maser RS*, et al.* SCF(FBW7) regulates cellular apoptosis by targeting MCL1 for ubiquitylation and destruction. Nature **2011**;471(7336):104-9 doi 10.1038/nature09732.

47. Wertz IE, Kusam S, Lam C, Okamoto T, Sandoval W, Anderson DJ*, et al.* Sensitivity to antitubulin chemotherapeutics is regulated by MCL1 and FBW7. Nature **2011**;471(7336):110-4 doi 10.1038/nature09779.

48. Terrano DT, Upreti M, Chambers TC. Cyclin-dependent kinase 1-mediated Bcl-xL/Bcl-2 phosphorylation acts as a functional link coupling mitotic arrest and apoptosis. Mol Cell Biol **2010**;30(3):640-56 doi 10.1128/MCB.00882-09.

49. Zhou L, Cai X, Han X, Xu N, Chang DC. CDK1 switches mitotic arrest to apoptosis by phosphorylating Bcl-2/Bax family proteins during treatment with microtubule interfering agents. Cell Biol Int **2014**;38(6):737-46 doi 10.1002/cbin.10259.

FIGURE LEGENDS

Figure 1. Neuroendocrine carcinomas originating in different organ sites share gene expression programs. **(A)** Heatmap showing relative transcript levels measured by RNA sequencing of AR-signature genes and NE-signature genes across patient metastases and cancer cell lines. ARPC, androgen receptor active prostate cancer; SCNPC, small cell neuroendocrine prostate cancer; MCC, Merkel cell carcinoma; SCLC, small cell lung cancer. **(B)** Multi-dimensional scaling analysis of samples across all genes measured by RNA-sequencing. **(C)** Heatmap of top 817 differentially expressed genes ($|\log_2$ fold change$|$ >4, FDR 0.05) in SCNPC vs. ARPC tumors with expression shown across all samples. **(D)** Heatmap of the expression 444 transcription factors differentially expressed between ARPCs and neuroendocrine cancers. **(E-G)** Expression levels of MYC family members across tumor subtypes determined by RNAseq (* indicates $p \leq 0.05$, ** = $p \leq 0.01$, *** = $p \leq 0.001$, **** = $p \leq 0.0001$ by Student's t-test).

Figure 2. Analyses of the druggable genome identifies BCL2 as a candidate therapeutic target in SCNPC. **(A)** Heatmap displaying genes in the druggable genome with differential expression between ARPCs and neuroendocrine tumors. **(B)** Expression of the transcript encoding the cell surface notch pathway gene DLL3 in **(B)** human tumors and **(C)** patient derived xenografts (PDX). **(D)** Expression of transcripts encoding BCL2 across tumor subtypes. **(E-G)** Boxplots depicting BCL2 transcript levels measured by RNAseq in metastatic tumors from patients with CRPC. **(H,I)** Pearson correlations between the neuroendocrine (NE) or androgen receptor (AR) signature score and gene expression. **(J)** Western Blot of selected BCL2 family members across a panel of cell lines. ARPC, AR program active prostate cancer; SCNPC, small cell neuroendocrine prostate cancer; SCLC, small cell lung cancer; MCC, Merkel cell carcinoma. * indicates $p \leq 0.05$, ** = $p \leq 0.01$, *** = $p \leq 0.001$, **** = $p \leq 0.0001$ by Student's t-test.

Figure 3. BCL2 antagonists inhibit the growth of SCNPC. **(A-D)** Dose response curves of BCL2-family inhibitors across a panel of prostate cancer cell lines. NCI-H660 and MSKCC EF1 are SCNPC, and LNCaP, C4-2, LAPC4, and VCaP are ARPC. **(E)** Western Blot for cleaved caspase-3 following 24 hour treatment with ABT-263 across the indicated cell lines. **(F)** BCL2 expression in ARPC versus SCNPC PDX models determined by RNAseq. $p = 0.011$ by Student's t-test. **(G)** Western Blot of selected BCL2 family members across a panel of prostate cancer PDX models. **(H)** Quantification of BCL2 staining of LuCaP TMA. (I)Scatterplot depicting Pearson correlation between the NE signature score and BCL2 gene expression in PDX lines. **(J)** Normalized tumor volumes of PDX models treated with vehicle control or ABT-263. ***$p<0.05$.

Figure 4. WEE1 inhibition can enhance the effects of BCL2 antagonism in SCNPC. **(A)** Boxplot of Wee1 expression across patient metastases and cell lines. ARPC, AR active prostate cancer; SCNPC, small cell neuroendocrine prostate cancer; MCC, Merkel cell carcinoma; SCLC, small cell lung cancer. (* indicates $p \leq 0.05$, **= $p \leq 0.01$, ***= $p \leq 0.001$, **** = $p \leq 0.0001$ by Student's t-test). **(B-D)** Boxplots showing WEE1 transcript expression measured by RNAseq in metastatic CRPCs in three independent studies. **(E,F)** Scatterplots depicting Pearson correlation between WEE1 transcript levels and NE signature score, or AR signature score. **(G)** Boxplot of WEE1 expression in ARPC and SCNPC PDX models of prostate cancer (p-value from Student's t-test). **(H,I)** Scatterplots depicting Pearson correlation between WEE1 transcript levels and NE signature score, or AR signature score. **(J,K)** Western Blots showing WEE1 protein levels across cell lines and LuCaP PDX models, respectively. **(L)** Quantification of WEE1 protein expression in LuCaP PDX lines. **(M)** Dose-response curves of AZD-1775 across a panel of prostate cancer cell lines. **(N)** Normalized tumor volumes of PDX models treated with vehicle control, ABT-263, AZD-1775 or the combination of ABT-263 and AZD-1775 or vehicle (bottom). *$p<0.05$; ***$p<0.001$.

Author Manuscript Published OnlineFirst on December 5, 2019; DOI: 10.1158/1078-0432.CCR-19-0775
Author manuscripts have been peer reviewed and accepted for publication but have not yet been edited.

Corella et al Figure 1

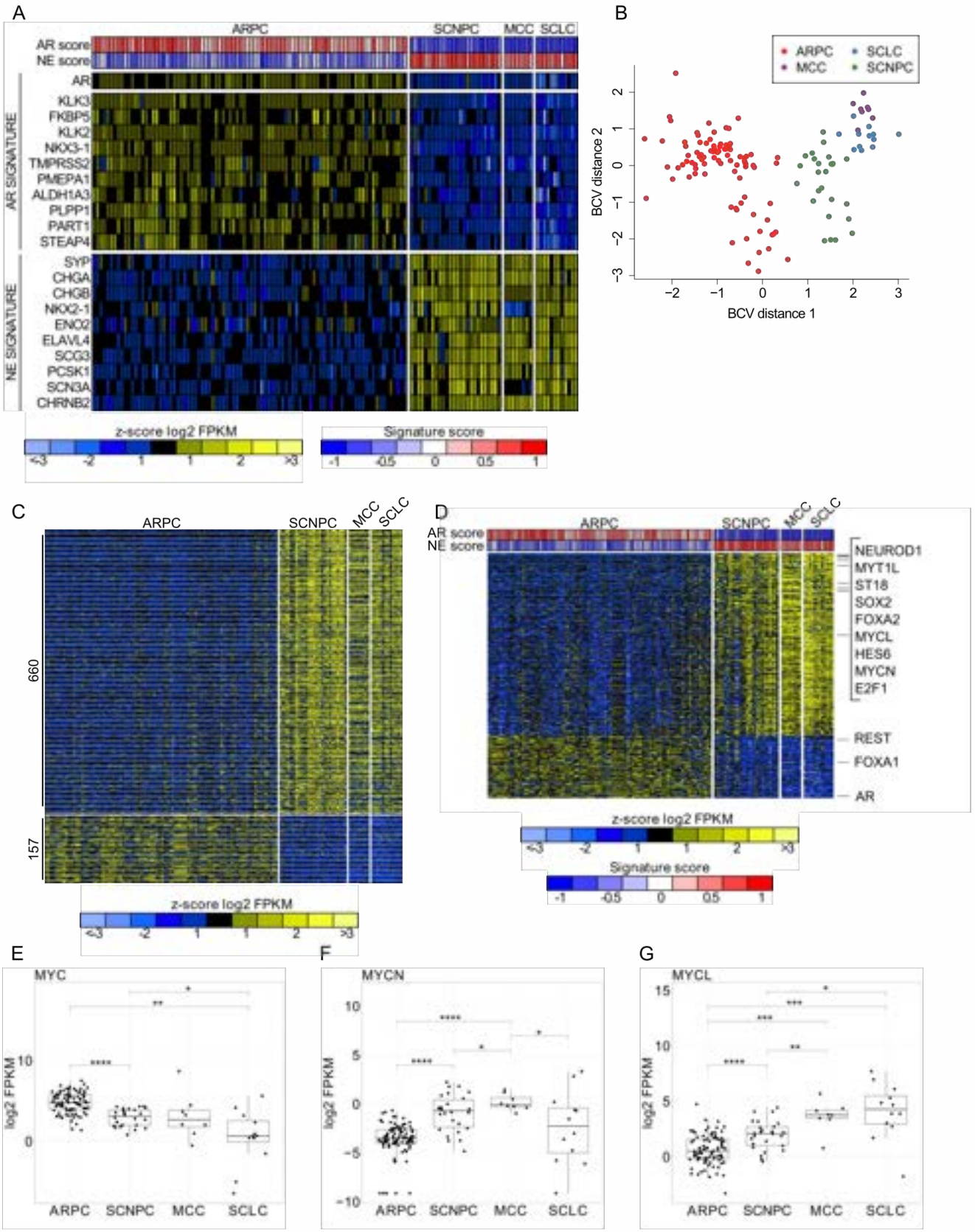

Author Manuscript Published OnlineFirst on December 5, 2019; DOI: 10.1158/1078-0432.CCR-19-0775
Author manuscripts have been peer reviewed and accepted for publication but have not yet been edited.

Corella et al Figure 2

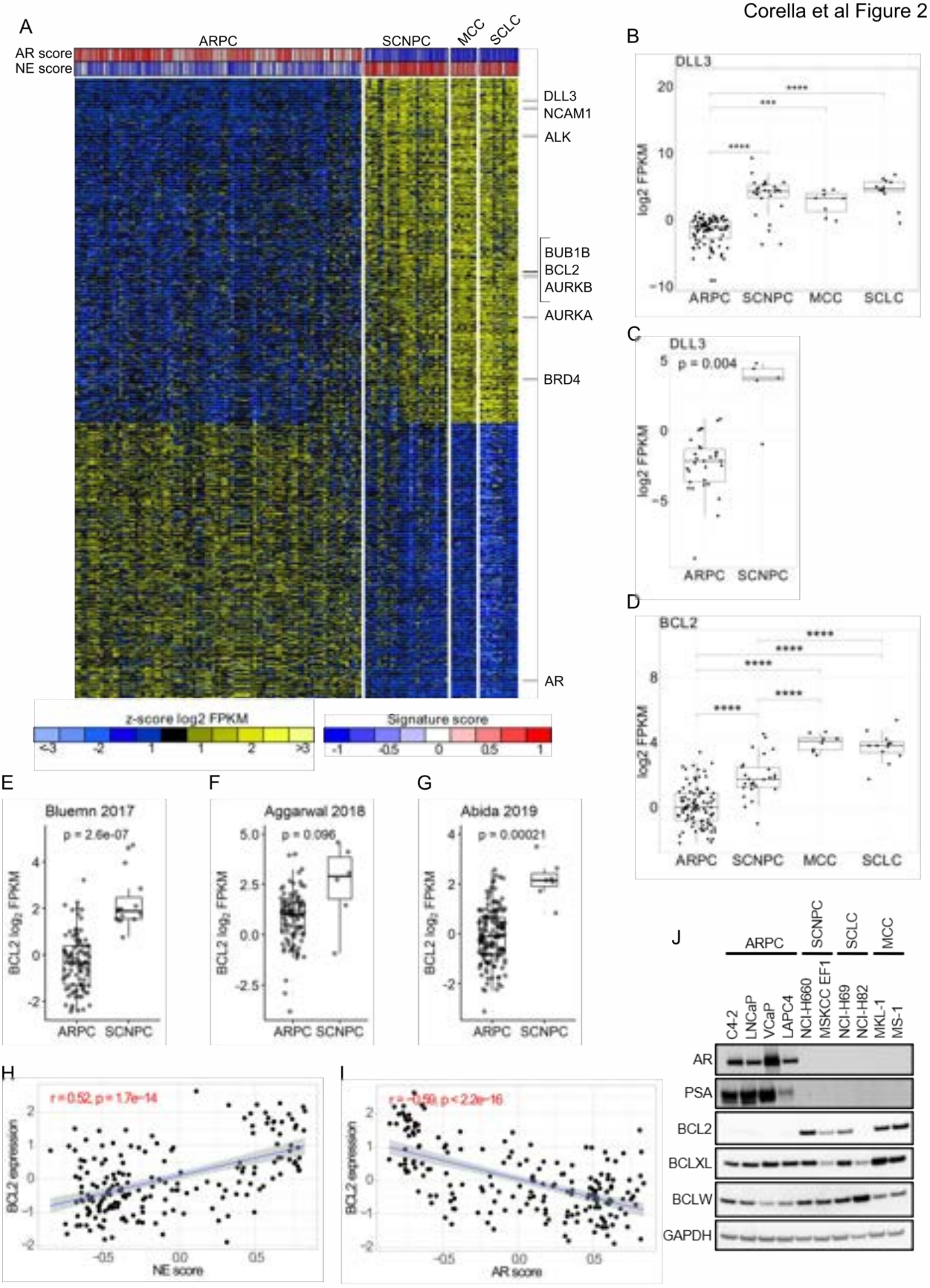

Author Manuscript Published OnlineFirst on December 5, 2019; DOI: 10.1158/1078-0432.CCR-19-0775
Author manuscripts have been peer reviewed and accepted for publication but have not yet been edited.

Corella et al Figure 3

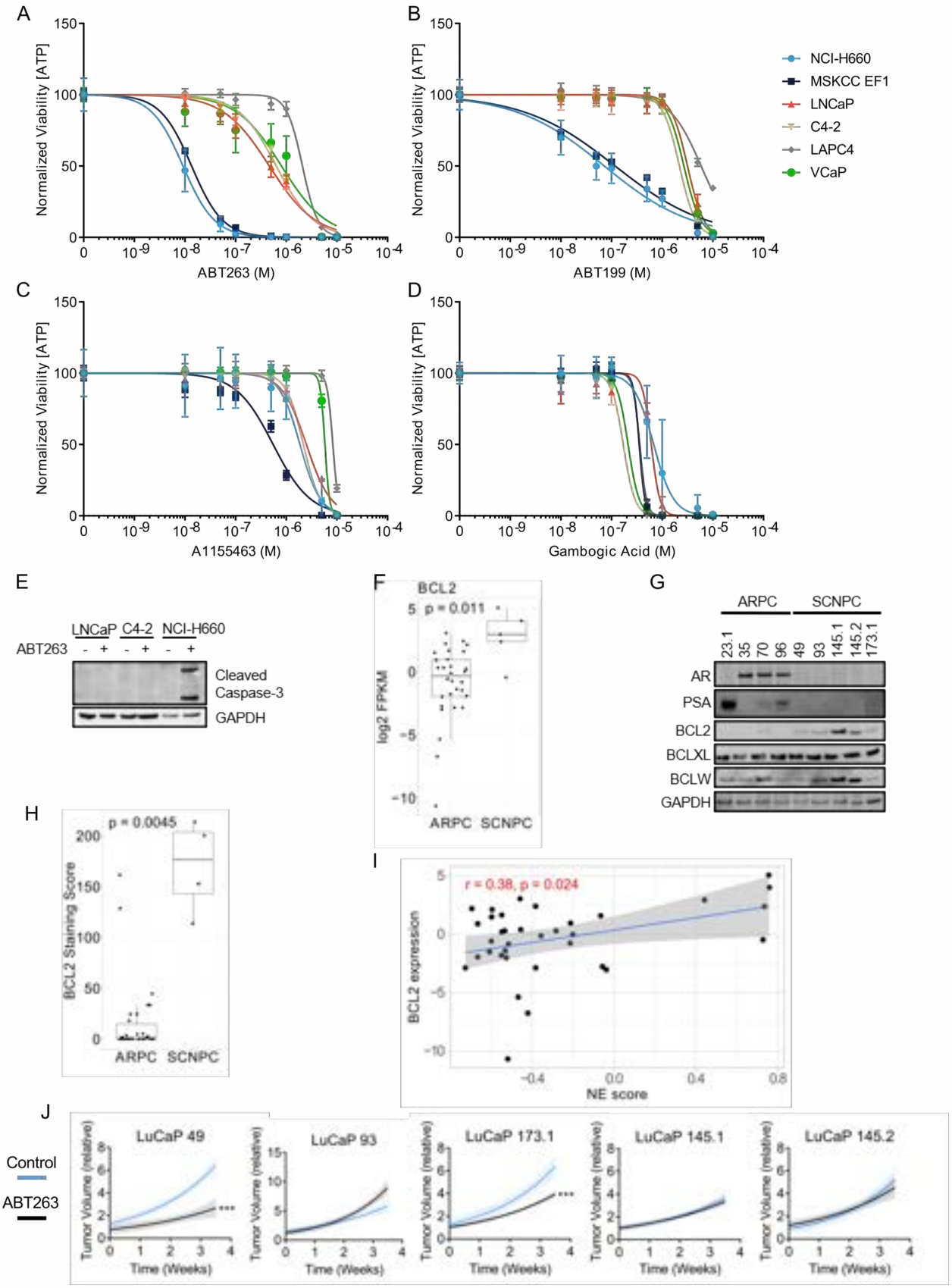

Corella et al Figure 4

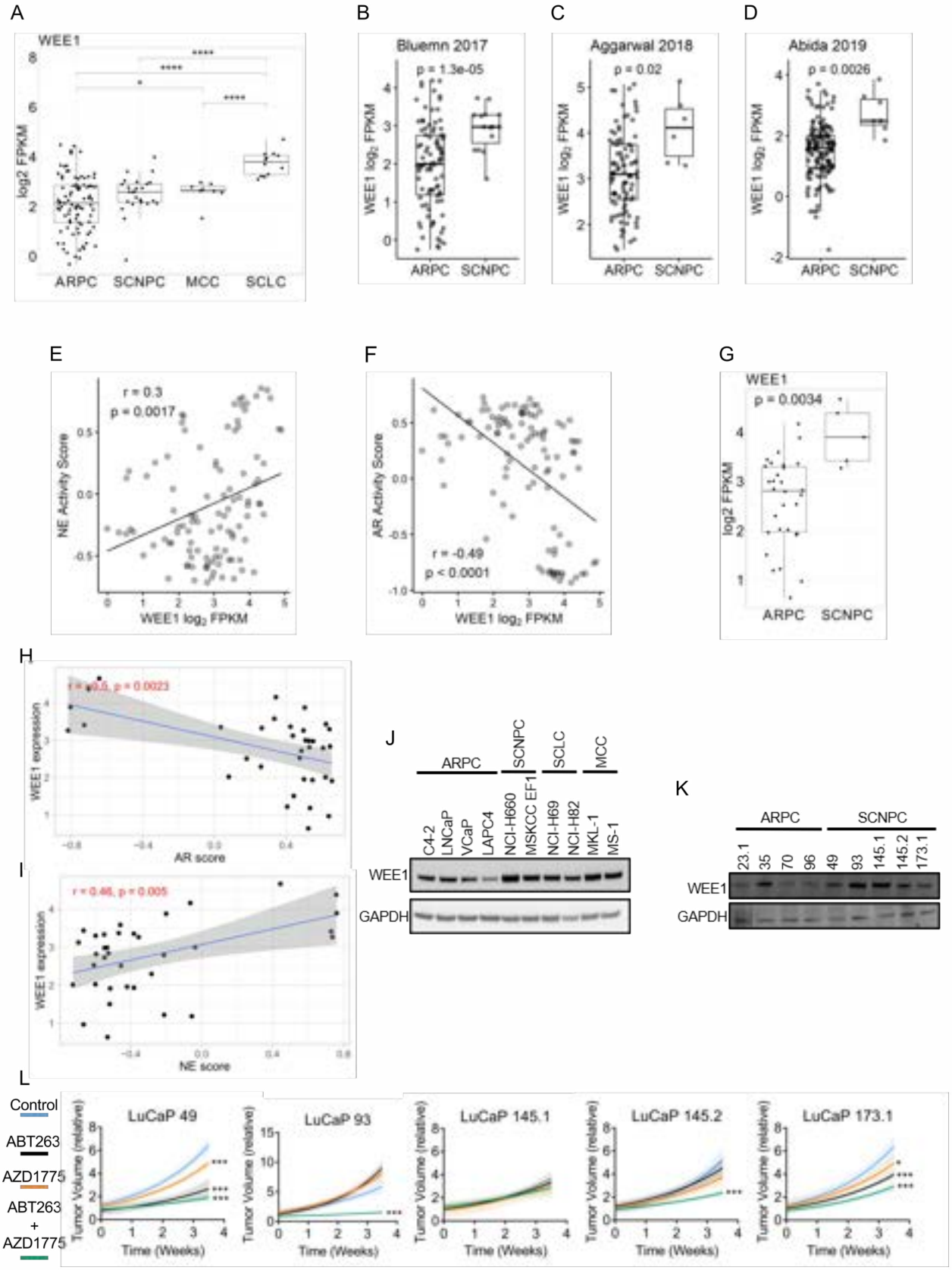

AACR American Association for Cancer Research

Clinical Cancer Research

Identification of Therapeutic Vulnerabilities in Small Cell Neuroendocrine Prostate Cancer

Alexandra N Corella, Ma Victoria Andrea Cabiliza Ordonio, Ilsa Coleman, et al.

Clin Cancer Res Published OnlineFirst December 5, 2019.